Shock-Ignition Experiments on OMEGA at NIF-Relevant Intensities

Shock ignition is a two-step inertial confinement fusion (ICF) concept in which a strong shock wave is launched at the end of the laser pulse to ignite the compressed core of a low-velocity implosion.[1] Two-step processes separate fuel assembly and ignition, relaxing driver requirements and promising high gains.[1,2] The gain of an ICF implosion can be significantly enhanced by launching a strong spherically convergent shock at the end of the compression (or assembly) pulse.[1,3–5] Another advanced-ignition concept is fast ignition,[6] which relies on a high-intensity, short-pulse laser generating an energetic beam of particles to trigger ignition. Shock ignition relies on highly shaped laser pulses, which might be produced by the pulse-shaping capabilities of the already operating National Ignition Facility (NIF).[7] Recent two-dimensional (2-D) simulations[4] have described shock-ignition designs with as low as 250 kJ of total laser energy. Proof-of-principle experiments[1,8] could be carried out at the NIF. The spherically convergent shock wave (ignitor shock) propagates through the shell during the coasting phase of the implosion and enhances the hot-spot compression, significantly improving the ignition conditions. The ignitor shock is launched at the end of the laser pulse by a spike with intensity in the range of 3×10^{15} to 10^{16} W/cm^2. This shock collides with the return shock near the inner shell surface. The return shock is the shock wave driven by the hot-spot pressure and propagating outward through the shell. After the ignitor and return shock collide, a third shock wave, resulting from the collision, propagates inward, leading to further compression of the hot spot. The final fuel assembly develops a centrally peaked pressure profile. Such non-isobaric assemblies exhibit a lower ignition threshold than standard isobaric assemblies. This mechanism is effective only in thick-shell implosions, where the ignitor shock wave significantly increases in strength as it propagates through the converging shell.[1]

Previous shock-ignition experiments[9] on OMEGA[10] studied fuel assembly with 60-beam symmetric implosions with 18 kJ of UV laser energy using 40-μm-thick, 0.9-mm-diam, warm surrogate plastic shells filled with deuterium gas of various pressures. The shock wave was launched by a spike in the laser power at the end of the pulse. The maximum intensity on target during the late power spike was $\sim 8 \times 10^{14}$ W/cm^2, and the resulting shock wave was relatively weak (the shock pressure was only 20 Mbar higher than the unshocked plasma pressure). These experiments showed a significant improvement in the performance of low-adiabat, low-velocity implosions compared to conventional implosions without a late spike in the laser pulse shape and showed that shock-wave timing is crucial to optimizing implosion performance. This shock-ignition campaign achieved the highest areal density ever measured on OMEGA (a neutron-rate–averaged areal density of 0.22 g/cm^2 and a peak areal density exceeding 0.3 g/cm^2) and neutron yields 4× larger than in conventional implosions.[9]

Parametric plasma instabilities[11] such as stimulated Brillouin scattering (SBS), stimulated Raman scattering (SRS), and two-plasmon-decay (TPD) instability are of concern in an ignition target design with spike-pulse intensities in the range of 10^{15} to 10^{16} W/cm^2 and full width at half maximum (FWHM) pulse durations of several hundred picoseconds. The instabilities increase the back-reflection of the laser light from the target, degrading the laser energy coupling to the capsule. They increase the fraction of the laser energy transferred to suprathermal electrons, a potential source of preheat that reduces the final core compression. In contrast to conventional hot-spot ignition, low-energy hot electrons generated during the power spike may have a positive effect on the implosions for shock ignition. The areal density increases rapidly during the final stages of the implosion. If the range of the hot electrons generated during the intensity spike is less than the shell thickness, they are stopped in the shell and augment the hydrodynamically driven shock wave. The effect of hot electrons on a shock-ignition target[12] was modeled in 1-D for a marginal igniting target using a multigroup diffusion model[13] for the hot electrons. The ignition window for a shock-launching time is considerably wider when the effects of moderate-energy hot electrons (a NIF-scale target can efficiently stop up to 150-keV electrons) are included, showing that hot electrons can indeed be beneficial for the shock-ignition scheme as long as their range is shorter than the shell's thickness.

This work provides the first measurements of parametric instability and preheat for conditions relevant for shock ignition (spherical target, long density scale length, and intensities above 2×10^{15} W/cm^2). Important physics issues including the hot-electron energy content, the hot-electron temperature, and laser backscattering for various intensities and time delays between fuel assembly and shock generation are studied. Switching from a 60-beam to a 40- plus 20-beam configuration with dual pulse shapes makes it possible to use tightly focused beams that generate a stronger shock compared to previous experiments. The data will help validate the shock-ignition target concepts at ignition-relevant intensities of ~5×10^{15} W/cm^2.

Figure 119.1 shows a schematic of the experiments described here. The compression pulse consisted of a shaped, low-adiabat laser pulse using 40 beams of OMEGA.[10] A late shock was driven by the remaining 20 beams that were delayed and focused on the compressed core to achieve intensities at the critical surface ranging from ~2×10^{15} to ~8×10^{15} W/cm^2. Plasma instabilities in density regions of up to quarter-critical density led to the generation of energetic electrons. Some of the fast electrons streamed into the hot core, heating it.

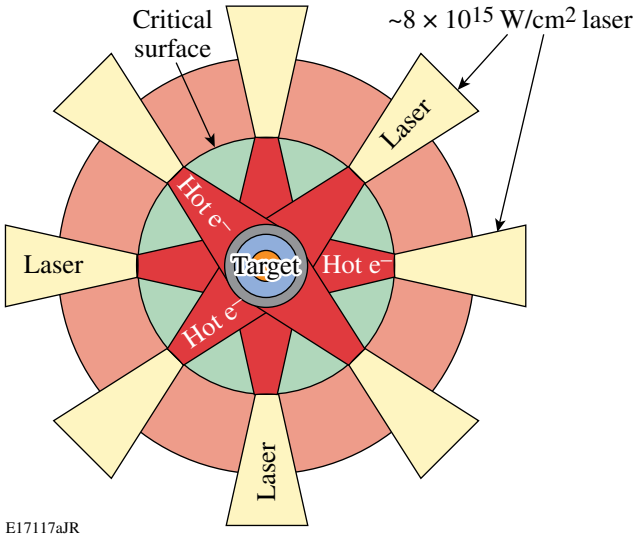

Figure 119.1
Schematic of the setup for studying laser–plasma interactions and preheating at high laser intensities relevant to shock ignition. Forty of the OMEGA laser beams implode the capsule at low intensities. Twenty delayed beams are tightly focused onto the critical density surface, where plasma instabilities lead to the generation of energetic electrons. Some of them will stream into the dense core.

The targets were 36-μm-thick, 430-μm-outer-radius, deuterated plastic (CD) shells coated outside with a 0.1-μm layer of aluminum and filled with D_2 gas with a pressure of ~30 atm. The capsules were imploded by 40 beams using a low-adiabat ($\alpha \sim 1.5$) pulse shape[14] at ~13.6 kJ of UV laser energy. The adiabat α is defined as the ratio of the plasma pressure to the Fermi pressure of a degenerate electron gas.[15] The solid curve in Fig. 119.2(a) shows the drive pulse shape comprising an ~100-ps (FWHM) Gaussian picket pulse preceding a shaped main-drive portion that consisted of a low-power foot and a moderate-power plateau with a total duration of 2.6 ns. The 351-nm-wavelength laser light of the 40 beams was smoothed with polarization smoothing[16] and distributed phase plates.[17] The delayed 20 beams (~4.6 kJ) that used an ~600-ps FWHM square pulse shape (dotted curve) were tightly focused on the shell without polarization smoothing or phase plates.

The experimental observables were the neutron yield,[18] the backscattered laser energy,[19] the hard x-ray signal,[20] and the neutron-rate–averaged areal density.[21] The laser light reflected back from the imploded capsule was measured from two beam ports [a shock-beam port (#25) and a drive-beam port (#30)], which were equipped with a full-aperture backscatter station (FABS).[19] The FABS measured the light backscattered into the final focusing lens aperture by down-collimating the reflection off the front surface of a full-aperture, uncoated glass wedge in the beamline onto a diagnostics table. Time-resolved spectra were recorded by two streaked spectrometers covering the wavelength ranges of 351±3 nm for SBS and 450 to 700 nm for SRS. The total backscattered energy in either of these spectral ranges was measured by calorimeters with an uncertainty of ±10%. The hard x-ray (HXR) signals (with photon energies >20 keV) were measured by the HXR detector with four channels measuring x rays >20, >40, >60, and >80 keV, respectively.[20] Areal densities (ρR) were inferred from secondary proton spectra.[21]

The delay time defined by the onset of the high-intensity beams with respect to the start of the drive pulse was varied from 2.3 to 2.9 ns. The effect on neutron and HXR yield is shown in Figs. 119.2(b) and 119.2(c) and on ρR in Fig. 119.2(d). The different symbols represent various focus conditions, where the number refers to the focus position in vacuum with respect to the shell's center. A negative number means that the focus is in front of the target toward the laser. The neutron yield increases by a factor of ~7 from 5×10^8 to ~3.5×10^9 for the shortest time delay. Two reference implosions with only the 40 drive beams produced neutron yields of 1.4×10^8 and 3.7×10^8; the solid line in Fig. 119.2(b) represents the average of both yields. The HXR yield's dependence on delay time is

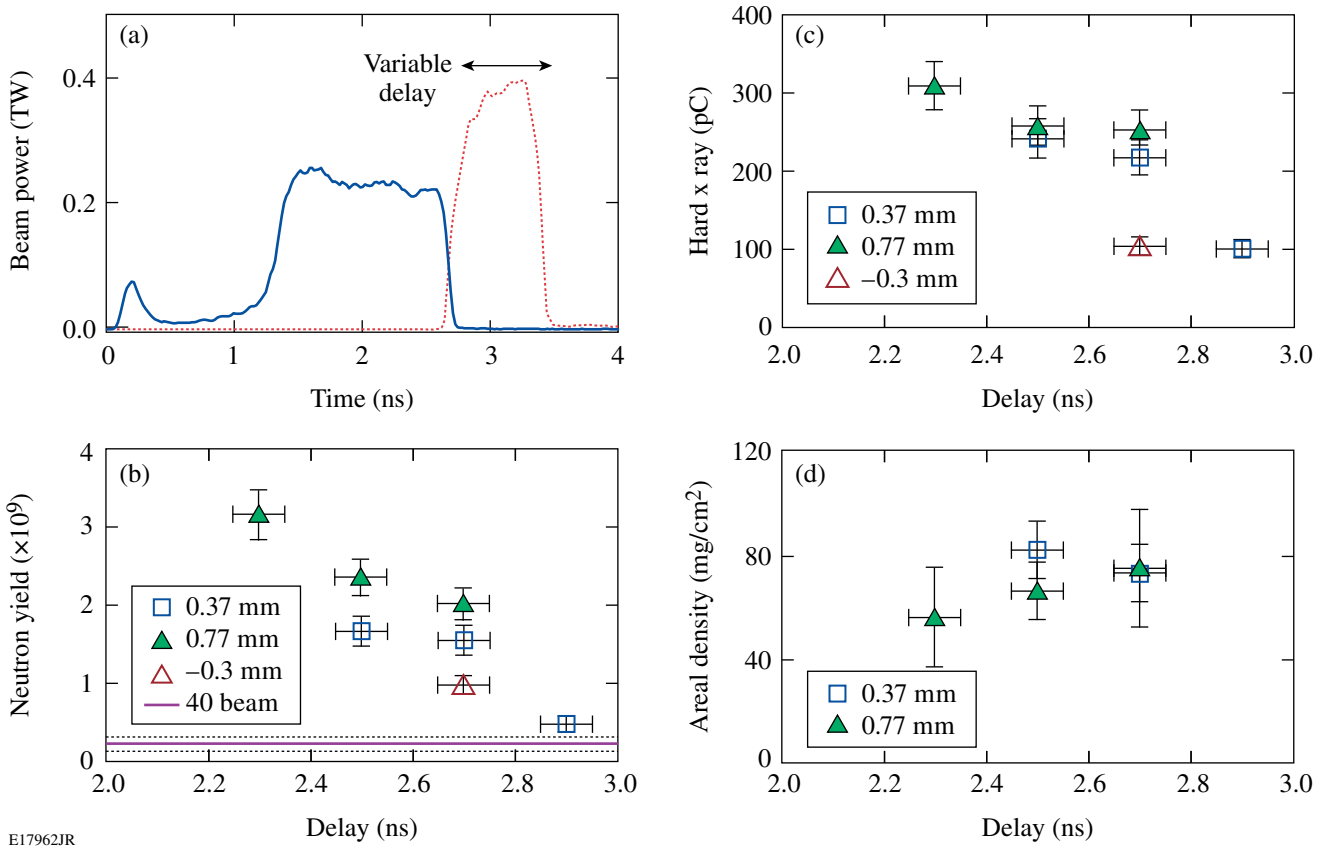

Figure 119.2
(a) Drive-pulse shape (solid) and high-intensity pulse (dotted), [(b)–(d)] measured neutron yield, hard x-ray yield, and neutron-rate–averaged areal density, respectively. The different symbols represent various focus positions with respect to the critical-density surface. The solid line in (b) is the average yield for 40-beam implosions and the dotted lines represent the error range. The 40-beam implosions produced no measurable HXR signal, and neutron yields were too low to obtain a ρR measurement.

similar. Figure 119.2(c) shows that signals measured by the >40-keV channel increase with shorter delay.

The HXR signal provided information on the hot-electron energy and temperature. Based on a calibration[22] of the hard x-ray detector, ~16±6% (~310-pC HXR signal) to ~5±2% of the shock-beam energy was converted into hot electrons. The conversion efficiency was highest for short delays when there was a partial overlap between the drive and shock pulses [Fig. 119.2(c)]. The hot-electron temperature was determined by fitting estimated values from the convolution of an exponentially decaying hard x-ray spectrum with the sensitivity of the different channels of the HXR detector to the measured four channels.[23] The inferred temperature was ~40 to 45 keV for all the shots, independent of laser intensity.

The implosions were nonuniform with a dominant $\ell = 2$ mode, which was caused by an unbalanced target illumination. The power imbalance was ~10.6%, given as the root-mean-square variation of the laser power on target. A typical value for a 60-beam symmetrical illumination on a spherical target is ~2% power imbalance.[24] The nonuniformity of the implosion is clearly seen in the x-ray pinhole camera image [Fig. 119.3(a)], which shows a strongly perturbed core with a 40-beam implosion. The core distortion was reduced when the 20 delayed, tightly focused beams were coupled into the target [Fig. 119.3(b)]. Figure 119.3(c) shows pinhole images from a symmetric implosion with a low-adiabat pulse shape and a similar target at a higher laser energy. Figures 119.2(b) and 119.2(c) show that despite large target illumination nonuniformity, a significant amount of the high-intensity pulse energy was coupled into the capsule, producing up to ~20× more neutrons and a strong HXR signal. The correlation of increasing neutron yield with a higher HXR signal suggests that the increased yield was partially due to hot electrons coupled into the outer regions of the compressing target. The late shock

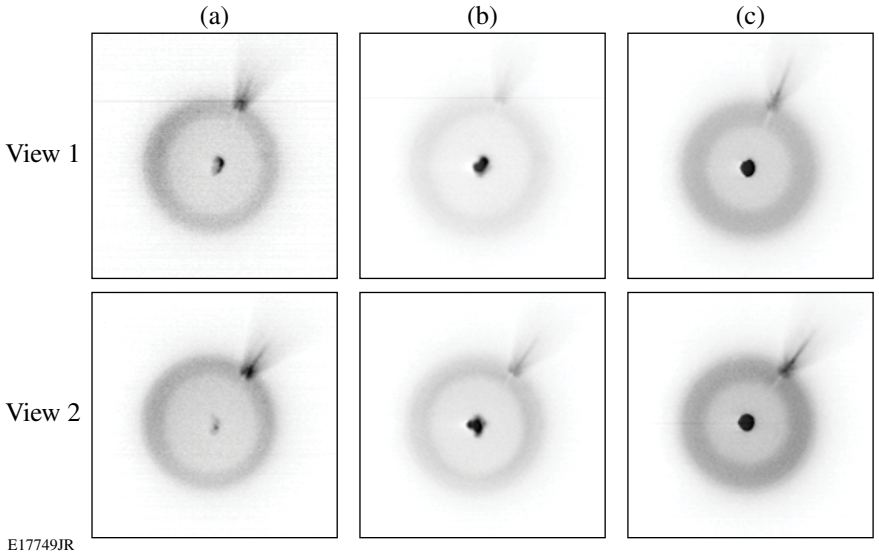

Figure 119.3
X-ray pinhole camera images from three different implosions. (a) Reference implosion with 40 drive beams, (b) 40- plus 20-beam implosion for a 0.77-mm focus position and a 2.3-ns time delay, (c) 60-beam uniform illumination. The feature at the upper right edge is due to the target stalk.

appears to be driven by a combination of the standard ablative and hot-electron drives.

The areal density does not change significantly with delay. The measured maximum ρR is 82±11 mg/cm^2, which is the average of four lines of sight, and the error bar is the standard deviation. This is ~30% lower than the expected ~115 mg/cm^2, which is scaled down from the measured 130±17 mg/cm^2 (Ref. 14) that was obtained with a more-uniform 60-beam implosion with the same fill pressure, the same adiabat, and an energy of 20 kJ and using the scaling of ρR with the laser energy to the power 1/3 (Ref. 14). For these shots, the standard deviation of the measured ρR varies from 15% to 35% of the mean ρR value, showing a large fluctuation of the areal density. The ρR degradation is most likely due to the strongly nonuniform implosion. Neutron yields from the 40-beam implosions were too low to obtain a ρR measurement.

The plasma reflectivity and HXR production from hot electrons were measured for various laser intensities. This was achieved through an intensity scan by shifting the focus of the 20 shock-driving beams relative to the shell's center. The nominal (in vacuum) laser intensity is quoted for the location of the critical-density plasma surface calculated by a 1-D hydrodynamic simulation.[13] The distance from the critical density to the capsule center was ~0.3 mm at 2.7 ns. For the lens position at –0.3 mm, the 20 beams were tightly focused on the critical-density location. The focus diameter of the 20 shock beams is estimated with ~80 μm, which gives a best-focus intensity up to ~8×10^{15} W/cm^2 for the shock beams in vacuum. The foci of the 20 shock beams did not overlap at the critical density for all lens positions used. No overlapped-beam effects[20] were expected and the HXR signal was dominated by single-beam interaction with the target.

Figure 119.4(a) shows the measured hard x-ray signal normalized to the estimated laser focus area versus lens position. The x-ray signal and consequently the hot-electron production increase with laser intensity presumably because of a larger growth in laser–plasma instabilities such as SRS and TPD, the primary sources of hot electrons.[20] Figure 119.4(b) shows the measured amount of laser backscatter energy of one shock beam (25) versus laser intensity. It increases from ~10% at ~2×10^{15} W/cm^2 to ~36% at ~8×10^{15} W/cm^2. The contribution from the SBS signal increases moderately from ~7% to 12%, while the SRS signal grows by almost a factor of ~5 from 5% to 24% and dominates the backscattering energy at the highest intensity. The simultaneously measured back-reflection through a neighboring drive-beam port (30) remained constant at the level of the implosions without the 20 shock beams for all beam delays and lens positions. This shows that the light from the shock beams was scattered back in a narrow cone and did not spill over into adjacent ports. No measurable signal of the 3/2 harmonic of the laser wavelength was measured for all inten-

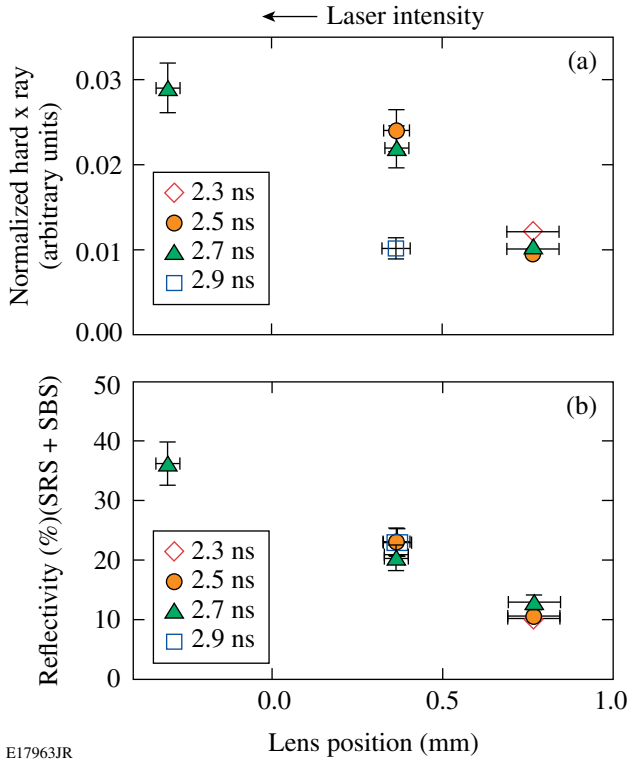

Figure 119.4
Measured (a) hard x-ray signal normalized to nominal beam focus area and (b) backscattered light versus lens focus position with respect to the shell's center. The laser intensity at the critical density is highest for the negative lens position corresponding to an intensity of $\sim 8 \times 10^{15}$ W/cm^2. The various symbols represent different time delays.

sities. The half-harmonic signal decreased by more than two orders of magnitude with higher intensities. At the maximum intensity, the half-harmonic signal was below the detection threshold, indicating no significant contribution of TPD to the hot-electron production. These experiments measured higher backscattering levels than other experiments at comparable laser intensities but different plasma conditions.[25] Measurements of parametric instabilities for indirect-drive–relevant ignition-plasma conditions with millimeter-density scale length and 15% critical-density targets report backscatter at 5×10^{15} W/cm^2 of up to 10%.[25] The absorbed energy rather than the backscattered light is the key issue. If 36% of the laser light is backscattered and 64% is absorbed, it represents a higher absorption fraction than the prediction of collisional absorption at these intensities (~40% to 50%). Because of the highly nonuniform plasma conditions and nonuniform illumination during the shock spike, the measurement of the scattered light through a few lines of sight cannot be used to infer the total absorbed fraction. In the pessimistic case where the predicted absorbed energy is reduced by the backscattered fraction, this can be remedied by an increase in spike power.

In conclusion, shock-ignition laser–plasma experiments in spherical geometry have been performed with nominal laser intensities of up to $\sim 8 \times 10^{15}$ W/cm^2. This was achieved by low-adiabat compression of warm plastic shells filled with D_2 gas by 40 beams and tightly focusing 20 beams on the compressed core. The additional 20 high-intensity beams enhanced the neutron yields by up to a factor of ~20, indicating a good coupling of the shock-beam energy to the core. A significant amount of backscattered laser energy from the high-intensity beams of up to 36% was measured at the highest laser intensity and about 20% at $\sim 5 \times 10^{15}$ W/cm^2. At high intensities, the back-reflection was dominated by SRS with some contribution from SBS but no significant contribution from TPD. About 10% of the high-intensity beam energy was converted into hot electrons. A hot-electron-energy distribution was generated with temperatures between ~40 and 45 keV, independent of laser intensity. This is beneficial for shock ignition since these electrons are stopped in a thin outer layer of the imploding target, augmenting the strong hydrodynamic shock. The reduction in driver energy caused by backscattering losses might be compensated by increasing the incident laser energy without the danger of preheating the target.

ACKNOWLEDGMENT

This work was supported by the U.S. Department of Energy Office of Inertial Confinement Fusion under Cooperative Agreement No. DE-FC52-08NA28302, the OFES Fusion Science Center grant No. DE-FC02-04ER54789, the OFES ACE FI grant No. DE-FG02-05ER54839, the University of Rochester, and the New York State Energy Research and Development Authority. The support of DOE does not constitute an endorsement by DOE of the views expressed in this article.

REFERENCES

1. R. Betti, C. D. Zhou, K. S. Anderson, L. J. Perkins, W. Theobald, and A. A. Solodov, Phys. Rev. Lett. **98**, 155001 (2007).

2. R. L. McCrory, D. D. Meyerhofer, R. Betti, R. S. Craxton, J. A. Delettrez, D. H. Edgell, V. Yu Glebov, V. N. Goncharov, D. R. Harding, D. W. Jacobs-Perkins, J. P. Knauer, F. J. Marshall, P. W. McKenty, P. B. Radha, S. P. Regan, T. C. Sangster, W. Seka, R. W. Short, S. Skupsky, V. A. Smalyuk, J. M. Soures, C. Stoeckl, B. Yaakobi, D. Shvarts, J. A. Frenje, C. K. Li, R. D. Petrasso, and F. H. Séguin, Phys. Plasmas **15**, 055503 (2008).

3. R. Betti and C. Zhou, Phys. Plasmas **12**, 110702 (2005).

4. X. Ribeyre *et al.*, Plasma Phys. Control. Fusion **50**, 025007 (2008).

5. A. J. Schmitt, J. W. Bates, S. P. Obenschain, S. T. Zalesak, D. E. Fyfe, and R. Betti, Fusion Sci. Technol. **56**, 377 (2009).

6. M. Tabak *et al*., Phys. Plasmas **1**, 1626 (1994).

7. E. I. Moses, J. Phys., Conf. Ser. **112**, 012003 (2008).

8. L. J. Perkins, R. Betti, K. N. LaFortune, and W. H. Williams, Phys. Rev. Lett. **103**, 045004 (2009).

9. W. Theobald, R. Betti, C. Stoeckl, K. S. Anderson, J. A. Delettrez, V. Yu. Glebov, V. N. Goncharov, F. J. Marshall, D. N. Maywar, R. L. McCrory, D. D. Meyerhofer, P. B. Radha, T. C. Sangster, W. Seka, D. Shvarts, V. A. Smalyuk, A. A. Solodov, B. Yaakobi, C. D. Zhou, J. A. Frenje, C. K. Li, F. H. Séguin, R. D. Petrasso, and L. J. Perkins, Phys. Plasmas **15**, 056306 (2008).

10. T. R. Boehly, D. L. Brown, R. S. Craxton, R. L. Keck, J. P. Knauer, J. H. Kelly, T. J. Kessler, S. A. Kumpan, S. J. Loucks, S. A. Letzring, F. J. Marshall, R. L. McCrory, S. F. B. Morse, W. Seka, J. M. Soures, and C. P. Verdon, Opt. Commun. **133**, 495 (1997).

11. W. L. Kruer, *The Physics of Laser–Plasma Interactions*, Frontiers in Physics, Vol. 73, edited by D. Pines (Addison-Wesley, Redwood City, CA, 1988).

12. R. Betti, W. Theobald, C. D. Zhou, K. S. Anderson, P. W. McKenty, S. Skupsky, D. Shvarts, V. N. Goncharov, J. A. Delettrez, P. B. Radha, T. C. Sangster, C. Stoeckl, and D. D. Meyerhofer, J. Phys., Conf. Ser. **112**, 022024 (2008).

13. J. Delettrez, R. Epstein, M. C. Richardson, P. A. Jaanimagi, and B. L. Henke, Phys. Rev. A **36**, 3926 (1987); M. C. Richardson, P. W. McKenty, F. J. Marshall, C. P. Verdon, J. M. Soures, R. L. McCrory, O. Barnouin, R. S. Craxton, J. Delettrez, R. L. Hutchison, P. A. Jaanimagi, R. Keck, T. Kessler, H. Kim, S. A. Letzring, D. M. Roback, W. Seka, S. Skupsky, B. Yaakobi, S. M. Lane, and S. Prussin, in *Laser Interaction and Related Plasma Phenomena*, edited by H. Hora and G. H. Miley (Plenum Publishing, New York, 1986), Vol. 7, pp. 421–448.

14. C. D. Zhou, W. Theobald, R. Betti, P. B. Radha, V. A. Smalyuk, D. Shvarts, V. Yu. Glebov, C. Stoeckl, K. S. Anderson, D. D. Meyerhofer, T. C. Sangster, C. K. Li, R. D. Petrasso, J. A. Frenje, and F. H. Séguin, Phys. Rev. Lett. **98**, 025004 (2007).

15. C. D. Zhou and R. Betti, Phys. Plasmas **14**, 072703 (2007).

16. T. R. Boehly, V. A. Smalyuk, D. D. Meyerhofer, J. P. Knauer, D. K. Bradley, R. S. Craxton, M. J. Guardalben, S. Skupsky, and T. J. Kessler, J. Appl. Phys. **85**, 3444 (1999).

17. Y. Lin, T. J. Kessler, and G. N. Lawrence, Opt. Lett. **21**, 1703 (1996).

18. V. Yu. Glebov, D. D. Meyerhofer, C. Stoeckl, and J. D. Zuegel, Rev. Sci. Instrum. **72**, 824 (2001).

19. W. Seka, D. H. Edgell, J. P. Knauer, J. F. Myatt, A. V. Maximov, R. W. Short, T. C. Sangster, C. Stoeckl, R. E. Bahr, R. S. Craxton, J. A. Delettrez, V. N. Goncharov, I. V. Igumenshchev, and D. Shvarts, Phys. Plasmas **15**, 056312 (2008).

20. C. Stoeckl, R. E. Bahr, B. Yaakobi, W. Seka, S. P. Regan, R. S. Craxton, J. A. Delettrez, R. W. Short, J. Myatt, A. V. Maximov, and H. Baldis, Phys. Rev. Lett. **90**, 235002 (2003).

21. F. H. Séguin, J. A. Frenje, C. K. Li, D. G. Hicks, S. Kurebayashi, J. R. Rygg, B.-E. Schwartz, R. D. Petrasso, S. Roberts, J. M. Soures, D. D. Meyerhofer, T. C. Sangster, J. P. Knauer, C. Sorce, V. Yu. Glebov, C. Stoeckl, T. W. Phillips, R. J. Leeper, K. Fletcher, and S. Padalino, Rev. Sci. Instrum. **74**, 975 (2003).

22. V. A. Smalyuk, D. Shvarts, R. Betti, J. A. Delettrez, D. H. Edgell, V. Yu. Glebov, V. N. Goncharov, R. L. McCrory, D. D. Meyerhofer, P. B. Radha, S. P. Regan, T. C. Sangster, W. Seka, S. Skupsky, C. Stoeckl, B. Yaakobi, J. A. Frenje, C. K. Li, R. D. Petrasso, and F. H. Séguin, Phys. Rev. Lett. **100**, 185005 (2008).

23. C. Stoeckl, V. Yu. Glebov, D. D. Meyerhofer, W. Seka, B. Yaakobi, R. P. J. Town, and J. D. Zuegel, Rev. Sci. Instrum. **72**, 1197 (2001).

24. F. J. Marshall, J. A. Delettrez, R. Epstein, R. Forties, R. L. Keck, J. H. Kelly, P. W. McKenty, S. P. Regan, and L. J. Waxer, Phys. Plasmas **11**, 251 (2004).

25. J. D. Moody *et al*., Phys. Rev. Lett. **86**, 2810 (2001).